Bio-mimetic Trajectory Generation Using a Neural Time-Base Generator

Yoshiyuki Tanaka and Toshio Tsuji
Department of the Artificial Complex Systems Engineering
Hiroshima University
Hiroshima, Japan

Vittorio Sanguineti and Pietro G. Morasso
Department of Informatics, Systems and Telecommunication
University of Genova
Genova, Italy

Received 19 May 2005; accepted 1 June 2005

This paper presents a neural time-base generator (TBG) that can generate a family of neural control signals with a controllable finite duration and bell-shaped velocity profile. Then, a bio-mimetic trajectory generation method using the neural TBG model is explained. Using the proposed model, the generation ability of human-like trajectories is examined through comparisons between computer simulations and human arm trajectories during reaching movements according to the curvature of constrained trajectories.

1. INTRODUCTION

We as individual human beings control our postures and movements according to tasks and environments, and show a great variety of skillful motions consciously or unconsciously. The movements demonstrated by the biological system appear to be roughly divided into rhythmic motions, such as walking and swimming, and one-shot motions, such as kicking and reaching. A great variety of skillful motions could be generated through serial and/or parallel combinations of rhythmic and one-shot motions. Many researches aiming at realizing these two primitive motion patterns have been actively conducted in both neurological and computational sciences.

Rhythmic behaviors are believed to be controlled by neural circuits located in the spinal cord or brainstem so-called Central Pattern Generator (CPG) that generates periodic neural motor commands.[1] The equations for the rhythmic pattern generator can be

Contract grant sponsor: Scientific Research Foundation of the Ministry of Education, Science, Sports and Culture, Japan.
Contract grant number: 15360226 and 16760203.

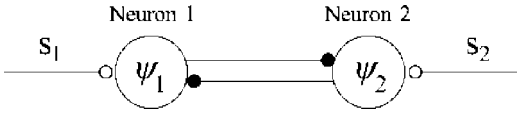

Figure 1. A mutual inhibition network of a CPG.

expressed by the half-centered oscillator model,[2] and Matsuoka formulated such neurological behaviors with a set of leaky integrators;[3]

$$T_a\dot{\psi}_i = -\psi_i - b_i\eta_i + s_i - w[\psi_j]^+, \tag{1}$$

$$T_b\dot{\eta}_i = -\eta_i + [\psi_i]^+, \tag{2}$$

where ψ_i is the state variable for the i-th individual neuron; b_i the parameter that determines the steady-state firing rate for a constant input; s_i the impulse rate of the tonic or slowly varying input; η_i the variable that represents the degree of fatigue or adaptation in the neuron; T_a and T_b time constants for the output ψ_i and the adaptation η_i, respectively; and $[\cdot]^+$ a threshold function that sets negative values to 0 while not affecting positive values. He also showed that mutual inhibition networks consisting of a few neurons as shown in Figure 1 can generate a variety of neural rhythmic signals under the specified condition of the parameters. The CPG model by Matsuoka has been widely utilized to regenerate rhythmic movements of animals on the basis of physiologically acquired evidences about its neural structure.[5–7] Recently, a biological controller inspired by the CPG model has been studied to make robots perform human-like rhythmic movements.[4–10]

On the other hand, there has been a well-known biological finding that a human usually moves his hand along a roughly straight path with a bell-shaped velocity profile between the specified two points.[11] As an explanation for such a human motor control mechanism underlining one-shot movements, many computational models have been proposed, such as a minimum jerk model,[12,13] a minimum torque-change model,[14] a minimum variance model,[15] and a VITE model.[16] The first to third models argue that the underlying mechanism is feedforward control with a criterion function, while the other considers it as feedback control by using external information detected from senses. All of these models can generate hand trajectories during free movements in a roughly good agreement with experimental data.

To the contrary, we have developed a trajectory generation approach using a time base generator (TBG) that generates a family of scalar signals with a controllable finite duration and bell-shaped velocity profile.[17–24] Our model is in the middle of the feedforward and feedback models: a human-like hand trajectory appears by synchronizing a translational and a rotational velocity of the hand with a neural time-base signal generated by a neuron network. In this paper, the neuron dynamics for outputting a neural time-base signal is formulated in the framework of the TBG model, and human arm movements constrained by a circular trajectory are focused on to discuss the effectiveness of the bio-mimetic control mechanism using the neural TBG. If such control mechanisms can be adopted into robot motion control, robots will be expected to be capable of more skillful motions, and can teach suitable human movements for patients with disabled motor functions.

This paper is organized as follows. Section 2 explains the concept of a neural TBG model, and presents a bio-mimetic trajectory generation method using neural TBG signals. Section 3 describes an experimental apparatus for constrained human arm movements with normal healthy subjects and shows a set of experimental results. In Section 4, computer simulations using the proposed trajectory generation method are carried out to demonstrate human-like hand trajectories with comparison of the experimental data.

2. A NEURAL TIME-BASE GENERATOR

A human acquires various kinds of skillful motions according to circumstances through experiences or practices in his/her lifetime, and we can visibly find such a skill acquisition process in the growth of a human infant.

For example, the normal infant has the capability of realizing smooth reaching movements with a bell-shaped velocity profile by the end of the fifth month.[25,26] Prior to that, he/she generates snaky spacial trajectories with a pulsating velocity profile that seems to be a combination of one-shot movements with a bell-shaped velocity profile as shown in Figure 2. Considering this fact, it is supposed that the control mechanism of human reaching movements involves a kind of CPG that is restructured to generate one-shot neural signals with a bell-shaped profile in the spinal cord or the brainstem.

The present paper defines such special CPG for

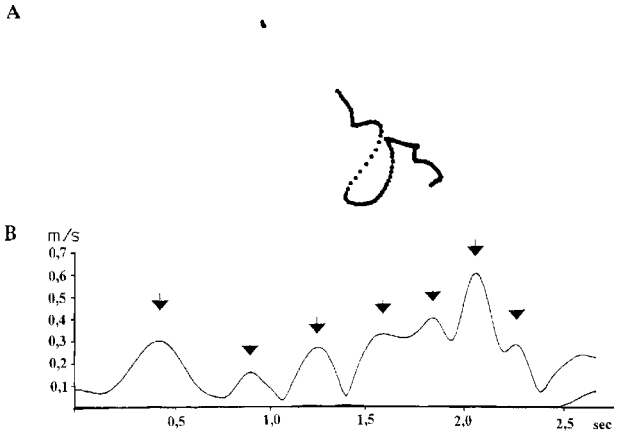

Figure 2. An example of the spatio-temporal trajectory during reaching movements of an infant at 4 months (ref. 25).

one-shot movements as a neural time-base generator, and formulates its dynamics from the neurological viewpoint in this section.

2.1. Neuron Model

A neuron is a nerve cell that outputs a nerve signal according to the received signals from other neurons, and is usually regarded as a multiple-input-single-output system. In this paper, we propose a specific model of neurons consisting of a multiplier, an integrator, and a power function as shown in Figure 3. The model outputs a signal ζ converted from the integrated signal of the product of inputs with the power function $\phi(\cdot)$, and its dynamics is formulated as

$$\dot{\xi}_i = \prod_{j=1}^{n} w_j \zeta_j, \tag{3}$$

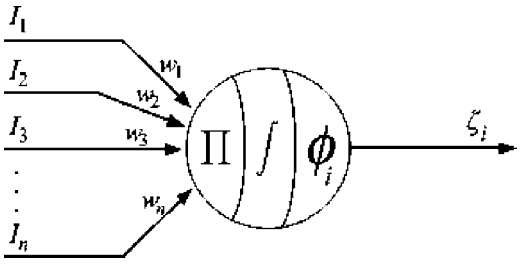

Figure 3. A schematic illustration of the proposed neuron element.

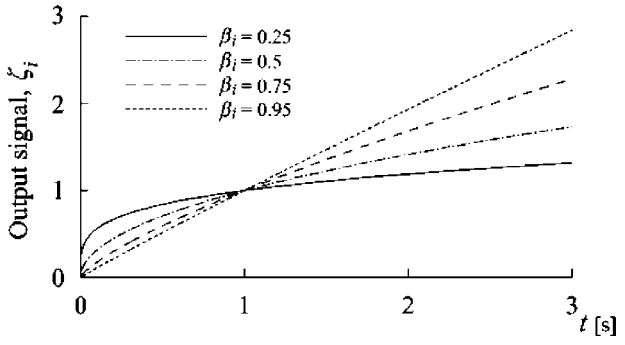

Figure 4. Step responses of the single neuron depending on β.

$$\zeta_i = \phi_i(\xi_i) \equiv \xi_i^{\beta_i}, \tag{4}$$

where ξ_i represents a membrance potential of the neuron body; w_j a weight coefficient determining firing rate for each input ζ_j; and β_i a time constant parameter under $0 < \beta_i < 1$.

Figure 4 shows responses of the single neuron to the step input from another neuron depending on the parameter $\beta_i = 0.25, 0.5, 0.75, 0.95$, where $n=1$, $w_1=1$, and $\xi_i(0)=0$. It can be seen that the output signal tends to rapidly close to 1 until 1 (s) as β_i decreases, while slowly increases after that. The response of the neuron changes according to values of the parameter β_i.

2.2. Neural TBG

The present paper proposes a simple reciprocal inhibitation network consisting of a couple of the neurons, as shown in Figure 5, which is called a *neural time-base generator* (neural TBG) model.

Let us consider the condition that $\xi_1(0) + \xi_2(0) = 1$ under the adequate normalization at the initial time. Dynamic behaviors of each neuron can be given as follows:

[Neuron 1]

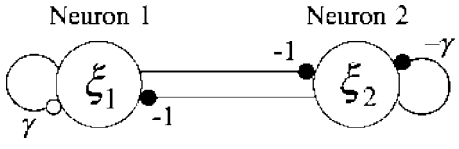

Figure 5. Neuron network of a neural time base generator.

$$\zeta_1 = \xi^{\beta_1}, \tag{5}$$

$$\dot{\xi}_1 = \gamma\zeta_1(-\zeta_2) = -\gamma\xi_1^{\beta_1}\xi_2^{\beta_2}, \tag{6}$$

[Neuron 2]

$$\zeta_2 = \xi^{\beta_2}, \tag{7}$$

$$\dot{\xi}_2 = -\gamma\zeta_2(-\zeta_1) = \gamma\xi_1^{\beta_1}\xi_2^{\beta_2}. \tag{8}$$

From (6) and (8), we have

$$\dot{\xi}_1 = -\dot{\xi}_2 \tag{9}$$

and thus yields

$$\xi_1(t) + \xi_2(t) = 1. \tag{10}$$

Substituting (10) into (6), dynamics of the state ξ_1 can be expressed as

$$\dot{\xi}_1 = -\gamma\xi_1^{\beta_1}(1-\xi_1)^{\beta_2}, \tag{11}$$

where γ is regarded as a parameter to determine both the speed and the finite time of a generating neural profile. This dynamics was originally defined for a control model of human arm movements with a bell-shaped velocity profile.[17]

There exist two singular points of the dynamic system; that is, $\xi_1 = 0$ and 1. It can be seen that the singular points are *Terminal attractor*.[27] Zak showed that a system with a terminal attractor always converges to the equilibrium point in a finite time t_f. The sufficient condition to have the terminal attractor is that the Lipschitz condition of ordinary differential equations is violated at the equilibrium point.

In the proposed neural TBG, the convergence time t_f is calculated from $\xi_1(0) = 1-\epsilon$ to $\xi_1(t_f)$ as[24]

$$t_f = \int_0^{t_f} dt = \frac{\Gamma(1-\beta_1)\Gamma(1-\beta_2)}{\gamma\Gamma(2-(\beta_1+\beta_2))} \tag{12}$$

where ϵ is a very small positive value, and $\Gamma(\cdot)$ the gamma function. Thus, the system converges to the equilibrium point $\xi_1(t_f)$ in the finite time t_f when γ in (12) is chosen as

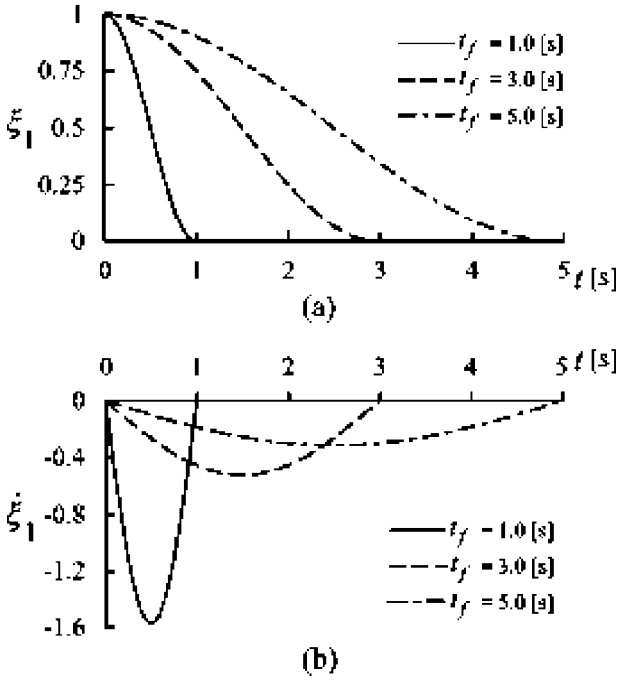

Figure 6. Time histories of ξ_1 and $\dot{\xi}_1$ depending on the specified convergence time t_f.

$$\gamma = \frac{\Gamma(1-\beta_1)\Gamma(1-\beta_2)}{t_f\Gamma(2-(\beta_1+\beta_2))}. \tag{13}$$

This means that the equilibrium point $\xi_1(t_f)$ is a terminal attractor that does not satisfy the Lipschitz condition: $|\dot{\xi}_1/\xi_1| \to \infty$.[27]

The velocity signal $\dot{\xi}_1(t)$ has a bell-shaped profile with the maximum absolute value, $|\dot{\xi}_1(t_f/2)| = \gamma 4^{-\beta}$, at $t = t_f/2$ under the condition with $\beta_1 = \beta_2 = \beta$. With regard to the acceleration profile, the following form can be derived as

$$\left|\frac{d^2\xi_1}{dt^2}\right| = |\gamma^2\{\beta_1 - (\beta_1+\beta_2)\xi_1\}\xi_1^{2\beta_1-1}(1-\xi_1)^{2\beta_2-1}| \tag{14}$$

and it can be seen that the condition for the existence of a bounded acceleration at the equilibrium point is given by the inequality $1/2 \leqslant \beta_i < 1$.[22–24]

Figure 6 shows time histories of ξ_1 and $\dot{\xi}_1$ according to the different specified convergence time $t_f = 1.0, 3.0, 5.0$ (s) under the parameter $(\beta_1, \beta_2) = (0.5, 0.5)$. While Figure 7 shows time histories of ξ

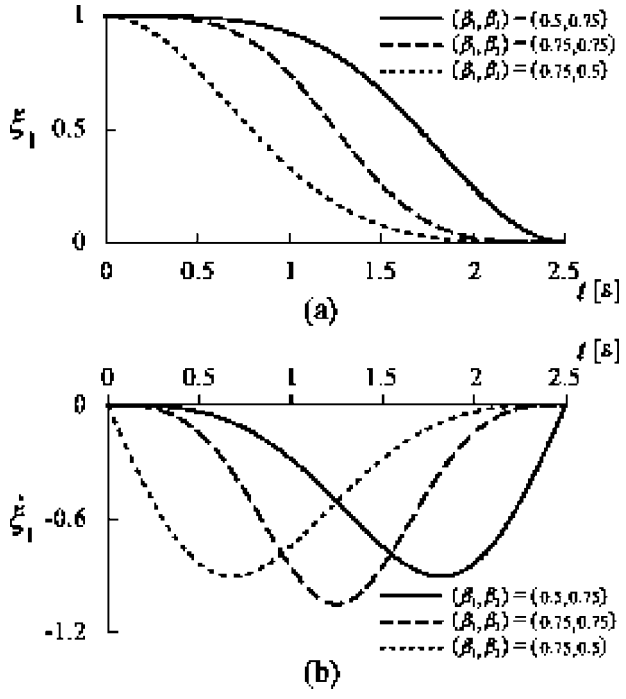

Figure 7. Time histories of ξ_1 and $\dot{\xi}_1$ depending on the adjustable parameter β_i.

and $\dot{\xi}$ using the parameters $(\beta_1, \beta_2) = (0.75, 0.5)$, (0.75, 0.75), and (0.5, 0.75) with the convergence time $t_f = 2.5$ (s). It can be seen that dynamics of the neural TBG signal can be regulated by changing the parameters t_f and β_i, so that the asymmetric profile as well as the symmetric profile can be generated with a controllable finite duration.

In summary, by selecting two parameters of the neural TBG (t_f and β), a family of time-varying signals $\xi(t)$ can be generated. In the next section, $\xi_1(t)$ is utilized to generate biomimetic trajectories. It should be noted that $\xi_2(t)$ can also be utilized when the trajectories with positive velocities are necessary.

2.3. Bio-mimetic Controller Using the Neural TBG

Figure 8 shows a block diagram of the proposed control mechanism using a neural TBG signal ξ, where X is the current position of the human hand and X_d the target point. This subsection explains a neural TBG model for a human-like trajectory generation method.

The bio-mimetic trajectory generation method for robots is based on the time scale transformation with the neural TBG in the framework of the artificial potential field approach (APFA).[21–24] The block diagram of the controlled robot can then be expressed by exchanging the pictorial shape of the human arm in Figure 8 with that of a robotic arm.

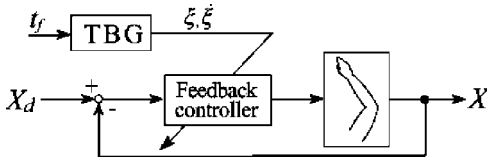

Figure 8. Block diagram of the TBG model for human arm reaching movements (refs. 18–24).

Generally, kinematic behaviors of a robot can be described as

$$\dot{X} = G(X)U \tag{15}$$

where $U \in \Re^n$ is the input motor command vector of a robot; and it is assumed that $\det G(x) \neq 0$. The relationship between actual time t and virtual time s is defined using the neural TBG signal $\xi(t)$ as

$$a(t) = \frac{ds}{dt} = -p\frac{\dot{\xi}}{\xi} \tag{16}$$

where a positive constant p is for regulating the degree of time compression; and a continuous function $a(t)$ is a kind of time scale function.[28] Note that the computational feasibility of the designed function $a(t)$ is lost at t_f since the denominator of $a(t)$ becomes zero ($\xi \rightarrow 0$). For the practical purpose, this problem can be avoided by introducing a very small positive constant parameter c into $a(t)$ as

$$a(t) = -p\frac{\dot{\xi}}{\xi + c}. \tag{17}$$

To simplify the discussion, theoretical expansion in the following part of this paper is carried out under the condition with $c = 0$. From (11) and (16), virtual time s can be derived as follows:

$$s = \int_0^t a(t)dt = -p \ln \xi(t). \tag{18}$$

It is obvious that virtual time s in (18) can be controlled by ξ, and never goes backward against actual time t. Thus, the system given in (15) can be rewrit-

ten in virtual time s defined by (18) as follows:

$$\frac{dX}{ds} = \frac{dX}{dt}\frac{dt}{ds} = G(X)U_s \tag{19}$$

where

$$U_s = \frac{1}{a(t)}U. \tag{20}$$

On the other hand, the APFA sets a potential function $V(X)$ which is minimized at a goal position X_d set in the task space. By applying a virtual attractive force to the goal position, the controlled robot can reach the target in infinite time. An example of such a feedback controller U_s can be designed as

$$U_s = -G^{-1}(X)\left(\frac{\partial V}{\partial X}\right)^T. \tag{21}$$

By using inverse time-scaling from virtual time s to actual time t for the feedback controller U_s in virtual time s, a feedback control law U in actual time t is derived as

$$U = -a(t)G^{-1}(X)\left(\frac{\partial V}{\partial X}\right)^T. \tag{22}$$

The system given in (15) converges the equilibrium point at the specified time t_f by the derived controller U in the actual time scale. That is, it is able to generate a spatio-temporal trajectory from the initial point X_0 to the target point X_d with the specified convergent time t_f.

2.4. Examples

Hand trajectories during human arm reaching movements in the 2D free space is examined using the proposed bio-mimetic trajectory generation method. A bio-mimetic controller for generating human-like trajectories during free movements can be designed as

$$U = -p\frac{\dot{\xi}}{\xi}(X_d - X) \tag{23}$$

with the potential function $V=1/2\,(X_d-X)^T(X_d-X)$ under the condition that $G(X)=I\in\Re^2$. With this controller, the translational velocity during reaching movements v_X is given by

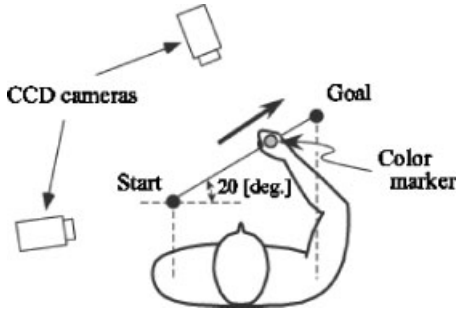

Figure 9. Experimental setup.

$$v_X = |\dot{X}| = \gamma p\,\xi^{\beta_1-1}(1-\xi)^{\beta_2}|X_d - X|. \tag{24}$$

It should be noted that the controller given in (23) can express the dispersion of traveling duration as well as the asymmetric property of velocity profiles by regulating the parameters t_f, β_1, and β_2.

On the other hand, Figure 9 shows the experimental apparatus for the measurement of reaching movements, where a stereo camera system (Quick MAG, Ouyou Keisoku Kenkyusyo Inc.) is employed that can detect a 3D position of a color marker attached at a measurement point (maximum of 8 points) from two 2D image sequences taken by two CCD cameras in real time (sampling rate: 60 (Hz)). In the experiments, a human subject was asked to move his right hand from the specified point to another.

Figure 10(a) shows examples of the experimental results for the subject, where the horizontal axis is the time and the vertical axis the translational velocity of hand movements. Note that all of the velocity profiles are single-peaked but there are some dispersions on the asymmetry of profiles. Accordingly, it should be modeled the control mechanism of reaching movements with consideration of such dispersions.

Figure 10(b) shows the human-like trajectories corresponding to the measured results in Figure 10(a), in which the values of β_i and t_f were set empirically under $p=1$. It can be found that the proposed method can be successfully expressed human-like trajectories including the dispersions observed in the empirical results by regulating the parameters of the neural TBG.

Summing up, the bio-mimetic approach using neural TBG can generate human-like trajectories during free movements including dispersion of movement time as well as asymmetric behavior of

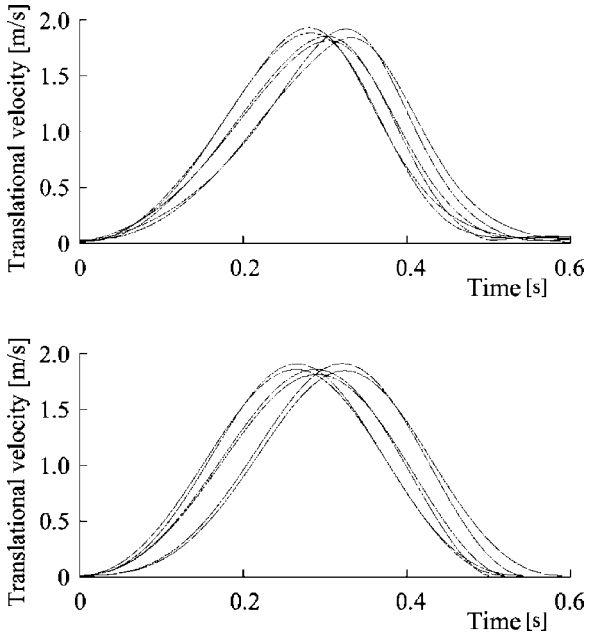

Figure 10. Comparison results of the simulated velocity profiles using a bio-mimetic controller with the human generated velocities.

hand velocity. However, most of human movements in daily activities are constrained from task environments during operational motion. The next section discusses a bio-mimetic trajectory generation in such constrained movements by a circular guide.

3. HUMAN HAND MOVEMENTS WITH CONSTRAINTS

3.1. Experimental Apparatus

Figure 11 illustrates an experimental system to examine human arm movements constrained by a circular trajectory. The system is composed of an impedance-controlled robot for providing virtual constraints to human hand movements, a computer for robot control and signal processing, and a display which indicates experimental results to a human subject. The robot is composed of two linear motor tables with one degree of freedom [Nihon Thompson Corp., maximum force ±10 (kg f); and Nihon Seikou Corp., maximum force ±40 (kg f)], which are placed orthogonally in order to realize the two-dimensional motion. A hand force generated by the subject is measured by a six-axis force/torque

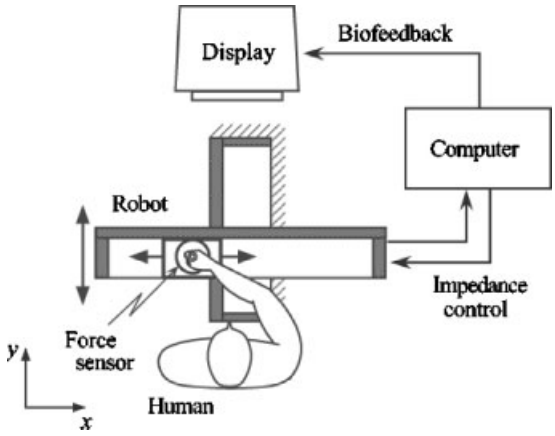

Figure 11. An overview of the experimental system.

sensor [BL Autotec Co. Ltd., resolution: force x and y axes, 0.05 (N); z axis, 0.15 (N); torque, 0.003 (Nm)] attached on the handle of the robot. Also, the handle position is measured by an encoder built in the linear motor table [resolution: Nihon Tomson Corp., 1.0 (μm); and Nihon Seikou Corp., 1.0 (μm)].

Figure 12 shows a control block diagram of the developed system to provide a virtual constrained trajectory with a constant curvature. The hand force $F_{ext}=[f_x,f_y]^T \in \Re^2$ in the Cartesian system Σ_c is transformed to the human hand force $F_p=[\tau,f_r]^T \in \Re^2$ expressed in the polar system Σ_p by

$$F_p = \begin{bmatrix} r\cos\left(\frac{\pi}{2}-\theta\right) & r\sin\left(\frac{\pi}{2}-\theta\right) \\ -\sin\left(\frac{\pi}{2}-\theta\right) & \cos\left(\frac{\pi}{2}-\theta\right) \end{bmatrix} F_{ext} \qquad (25)$$

where r is the radius of a circular constrained trajectory. The origin of the polar system Σ_p is set at the rotational center determined by the initial and target points with the specified radius r. Also, θ is defined as the rotational angle from the x axis; τ the torque equivalent to the tangential element of the hand

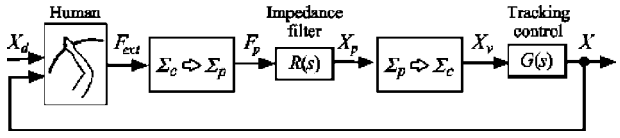

Figure 12. Block diagram of the impedance controlled system for virtual constrained movements.

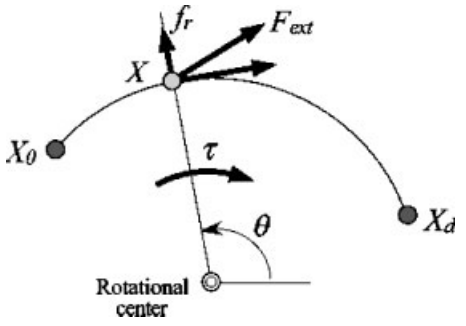

Figure 13. Coordinate transformation of hand force.

force F_{ext} for the trajectory; and f_r the normal element of F_{ext} (see Figure 13). The impedance-control part outputs a virtual target position of the robot handle in the polar system Σ_p, $X_p=[r_p, \theta_p]^T \in \Re^2$, from the hand force F_p by the following dynamics of the impedance-controlled robot:

$$M\ddot{X}_p + B\dot{X}_p + KX_p = F_p \tag{26}$$

where $M=\mathrm{diag}(M_\theta, M_r)$, $B=\mathrm{diag}(B_\theta, B_r)$, $K=\mathrm{diag}(K_\theta, K_r) \in \Re^{2\times 2}$ are the diagonal matrices of robot inertia, viscosity, and stiffness properties, respectively. The first element of each matrix is an impedance parameter for the tangential direction of the trajectory while the second one is for the normal direction. The tracking part works to make the robot handle follow to the virtual target $X_v=[r_p \cos\theta_p, r_p \sin\theta_p]^T \in \Re^2$ expressed in the Cartesian system Σ_c. By installing the above control algorithm into the developed system, a various kind of virtual constrained trajectories can be produced.

3.2. Experimental Method

A human subject is asked to move the handle of an impedance-controlled robot by his right upper arm from the specified two points. A set of experiments was carried out for five normal subjects (male university students aged 22–24).

Figure 14 shows the experimental conditions designed by referring to the literature,[14] in which points T1, T2, …, T6 represent the specified initial/target points of human arm movements and the origin of the Cartesian coordinate Σ_c agrees with the shoulder point of a human subject. Spatio-temporal trajectories between the specified two points were measured for the different curvatures $\rho=1/r$ $=0.0, \pm 2.0, \pm 4.0\ (\mathrm{m}^{-1})$ for seven different paths, path-a, path-b, …, path-g, described as in Figure 14. The curvature for path-c was setting as $\rho=0.0, \pm 2\ (\mathrm{m}^{-1})$ because of the motion range of the experimental system.

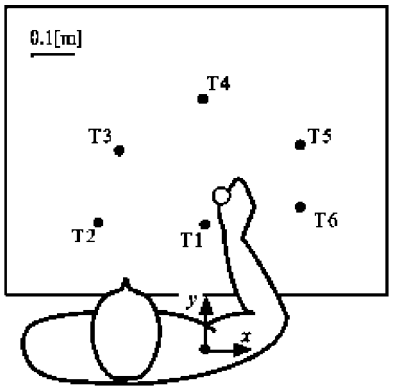

Path-a: T3 → T5, Path-b: T3 → T6, Path-c: T2 → T6
Path-d: T1 → T3, Path-e: T4 → T1, Path-f: T4 → T6
Path-g: T5 → T3

Figure 14. Experimental conditions of the specified initial and target points.

Robot impedance properties of the tangential direction to hand motion were set as $(M_\theta, B_\theta, K_\theta)$ $=[1.5\ r^2\ (\mathrm{Kg\,m^2}), 30\ r^2\ (\mathrm{Ns\,m}), 0\ (\mathrm{Nm})]$, while ones of the normal direction as (M_r, B_r, K_r) $=[100\ (\mathrm{Kg}), 2000\ (\mathrm{Ns/m}), 10000\ (\mathrm{N/m})]$ to provide a virtual constraint for the subject's hand movements.

3.3. Experimental Results

Figures 15 and 16 show the typical results of the spatio-temporal trajectories generated by Subject A under the conditions of path-b and path-f, respectively, where the hand velocity profiles of four trials are plotted in the panels (b)–(f) depending on the specified curvature. The hand velocity profile has a single-peak for the straight constrained trajectory ($\rho=0$), while the velocity profile becomes asymmetric as the curvature of trajectories increases. Note that a double-peaked profile does not always appear even when the curvature is set at the maximum curvature $[|\rho|=4\ (\mathrm{m}^{-1})]$ within the experimental conditions in this paper.

Table I shows the overall results for all subjects describing the type of velocity profiles according to the specified conditions. It can be found that the subjects generated a double-peaked velocity profile under the conditions of path-a, path-b, and path-g with

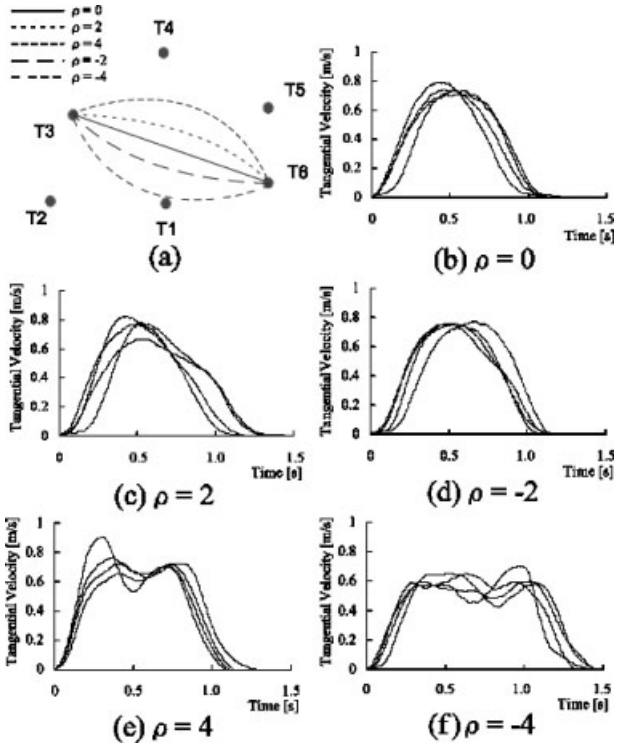

Figure 15. Generated trajectories and tangential velocities of the end-point (path-b: T3 → T6).

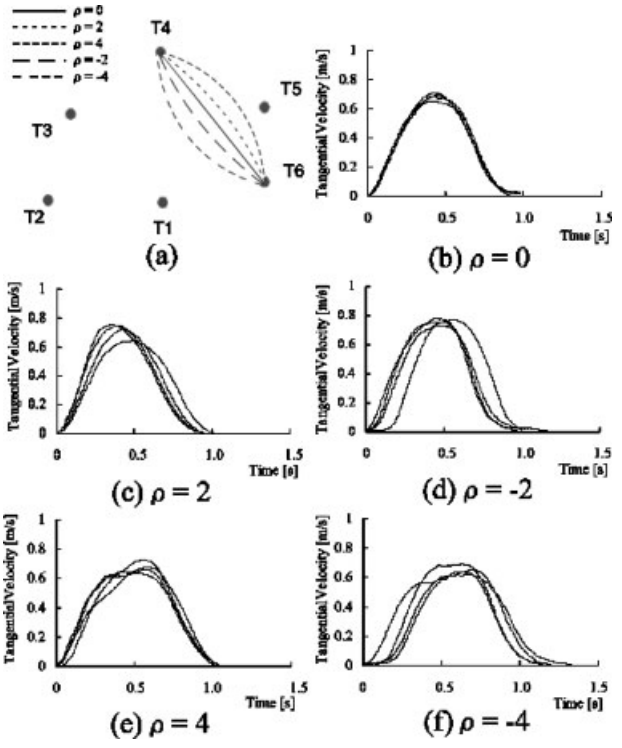

Figure 16. Generated trajectories and tangential velocities of the end-point (path-f: T4 → T6).

a large curvature in which the constrained trajectory was across the front of their bodies. Accordingly, the translational velocity of hand movements is affected by both the curvature of spatial trajectories and the relative position between initial and target points.

4. BIO-MIMETIC TRAJECTORY GENERATION FOR ROBOTS

4.1. Bio-mimetic Trajectories for Rehabilitation Robots

Recently, a number of training and rehabilitation systems using robots have been developed. Especially, to support joint motion exercises for prevention and improvement of joint contraction and muscle atrophy, many kinds of a continuous-passive-motion (CPM) device, which moves joints of a patient passively, have been developed.[29–32] However, in these previous training systems, it is difficult to offer efficient training for realizing a smooth motion like a healthy person produces because time-related characteristics of motion such as a velocity profile and a movement time are not used as a training goal.

On the other hand, we have proposed a bio-mimetic rehabilitation robot for reaching movements by using the TBG model with the robot control system as shown in Figure 17.[22] The training system is constructed in such a way that a trainee operates an impedance-controlled robotic device during training while the robot evaluates and assists the trainee's movements with the assisting force F_{aid} on the basis of the given human-like trajectory X_r that is generated using the TBG. Accordingly, it is expected that the training considering normal dynamic behaviors of human movements can be provided to a trainee.

The rest of this section discusses human-like trajectories constrained by a circular guide to transform the developed experimental system shown in Figure 11 into a bio-mimetic rehabilitation robot for training human motor control abilities during constrained movements.

Table I. Type of the velocity profiles depending on the experimental conditions.

	ρ	Subject A	Subject B	Subject C	Subject D	Subject E
Path-a	−4	D	D	S	D	D
T3→T5	−2	S	D	S	S	S
	0	S	S	S	S	S
	2	S	S	S	S	S
	4	S	S	S	D/S	S
Path-b	−4	D	D	S	D/S	D
T3→T6	−2	S	D/S	S	D/S	D/S
	0	S	S	S	S	S
	2	S	S	S	S	S
	4	D	D/S	S	S	S
Path-c	−2	S	S	S	D/S	D
T2→T6	0	S	S	S	S	S
	2	S	S	S	S	S
Path-d	−4	S	S	S	S	S
T1→T3	−2	S	S	S	S	S
	0	S	S	S	S	S
	2	S	S	S	S	S
	4	S	S	S	D/S	S
Path-e	−4	S	S	S	S	S
T4→T1	−2	S	S	S	S	S
	0	S	S	S	S	S
	2	S	S	S	S	S
	4	S	S	S	S	S
Path-f	−4	S	S	S	S	S
T4→T6	−2	S	S	S	S	S
	0	S	S	S	S	S
	2	S	S	S	S	S
	4	S	S	S	S	S
Path-g	−4	D/S	S	S	D/S	D/S
T5→T3	−2	S	S	S	S	S
	0	S	S	S	S	S
	2	S	S	S	S	S
	4	D	D/S	S	D	D/S

D: Double peak, S: Single peak.

4.2. Trajectory Generation by a Bio-mimetic Controller

To utilize the constructed control system as shown in Figure 12, a bio-mimetic controller is designed in the polar system Σ_p in this paper. Then, to express the family of curved trajectories with a double-peak velocity profile, a virtual via-point $X_{vp} \in \Re^2$ is set on the task space as a time-varying equilibrium point of the potential field as shown in Figure 18. The virtual via-point starts moving at time t^a and reaches the final point at time t^b by synchronizing the dynamics of θ_v with a neural TBG signal ξ_v.

The bio-mimetic controller using the neural TBG, $v_\xi \in \Re^2$, can be designed as

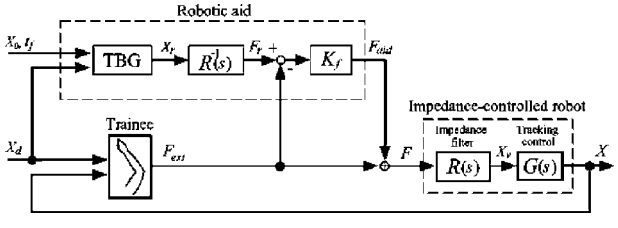

Figure 17. Block diagram of a bio-mimetic rehabilitation robot (ref. 22).

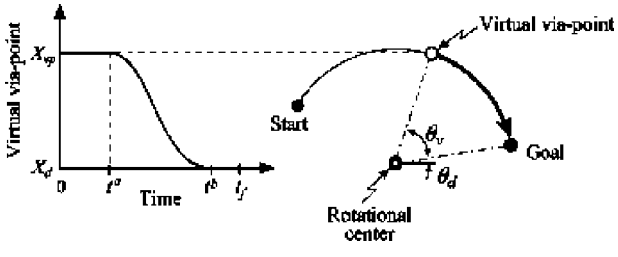

Figure 18. Virtual via-point used in the simulations.

$$v_\xi = -r\frac{pk_\theta\dot{\xi}}{2\xi}\{(\theta_d - \xi_v\theta_v) - \theta\}\begin{bmatrix}\cos\left(\frac{\pi}{2}-\theta\right)\\ \sin\left(\frac{\pi}{2}-\theta\right)\end{bmatrix} \quad (27)$$

with the following potential function V_θ in the polar system Σ_p

$$V_\theta = \frac{k_\theta}{2}(\theta_d - \theta)^2 \quad (28)$$

where θ_d is the angle of the target point X_d in the polar system.

When the virtual via-point is not set at the task space, the time derivative of V_θ yields

$$\dot{V}_\theta = \left(\frac{\partial V_\theta}{\partial\theta}\right)^T\frac{|v_\xi|}{r} = pV_\theta\frac{\dot{\xi}}{\xi} < 0. \quad (29)$$

As $\dot{V}_\theta$ is always negative except at the equilibrium point, the system of the end-point in the actual time scale is asymptotically stable. Moreover, this differential equation given in (29) can be readily solved as follows:

$$V_\theta = V_\theta(0)\xi^p. \quad (30)$$

It can be seen that the potential function V_θ is "synchronized" with the neural TBG signal because V_θ is proportional to the pth power of ξ. Accordingly, the end-point is bound to reach the target position X_d from the initial position X_0 just at $t=t_f$ by using the controller v_ξ in (27).

When the virtual point X_{vp} is set in the task space, the potential filed by V_θ varies according to the dynamic behaviors of X_{vp}. As far as X_{vp} converges to the target point X_d before the specified time t_f under $V_\theta<0$, it can be done the same discussion with the case when no virtual via-point is set: That is, the end-point is bound to reach the target position just at $t=t_f$.

Figure 19 shows examples of the simulated human-like trajectories in the case of path-b corresponding to the experimental results presented in Figure 9, in which a white circle represents the initial position of a virtual via-point X_{vp} and a dotted line in the panels (c), (e), and (f) shows the velocity without setting a virtual via-point. The parameters for the designed controller and the virtual via-point were determined to realize a suitable velocity profile

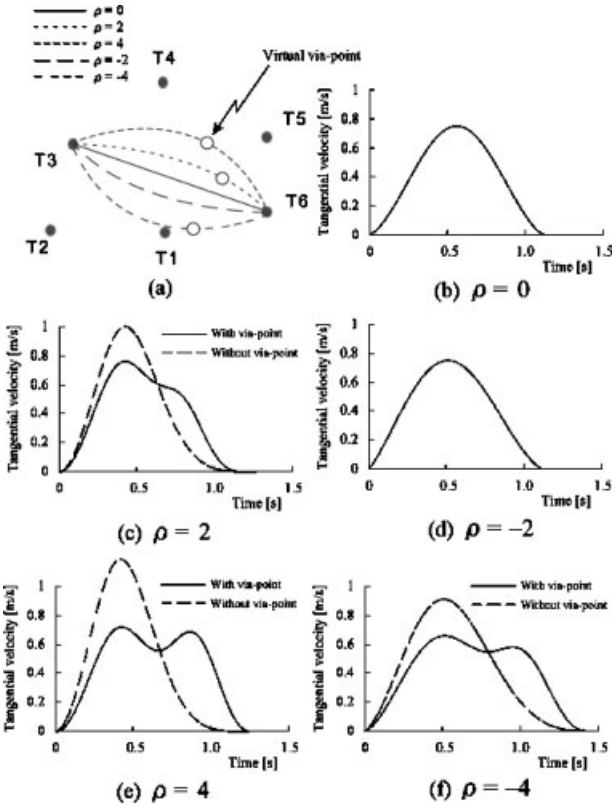

Figure 19. Simulated trajectories and tangential velocities of the end-point (path-b: T3→T6).

according to the curved trajectories under the condition with $p=1.0$ and $k_\theta=1.0$ as shown in Table II. It can be seen that the simulated trajectories have the similar characteristics to the observed human trajectories: the velocity profile tends to be double-peaked as the curvature increases. However, without setting the via-point, the velocity profiles are always single-peaked with difference from the empirical results by the human subjects. It supposes that a human utilizes such a virtual via-point to avoid generating surplus hand force toward the constrained direction.

Consequently, the designed controller using the neural TBG can generate human-like trajectories with the kinematic features of human arm movements constrained by a circular trajectory by utilizing a virtual via-point.

5. CONCLUSION

The present paper has presented the neural TBG model outputting a neural signal with bell-shaped

Table II. Specified parameters for the designed controller and the virtual via-point.

Curvature	Controller			Virtual via-point				
ρ	t_f	β^1	β^2	t^a	t^b	β_v^1	β_v^2	θ_v
4	1.25	0.8	0.65	0.3	1.3	0.75	0.75	$2/5\theta_d$
2				0.3	1.1	0.75	0.75	$1/4\theta_d$
0	1.125	0.6	0.6			—		
−2	1.125	0.6	0.55					
−4	1.5	0.75	0.6	0.4	1.4	0.75	0.75	$2/7\theta_d$

profile and the bio-mimetic trajectory generation method for generating human-like trajectories. Then, human arm reaching movements constrained by a virtual circular guide were examined with the normal subjects according to the position of initial and target points and the curvature of guides. The experimental results demonstrated that the translation velocity profile of the human hand tends to be double-peaked when the circular path with large curvatures closes to the human body. By applying the TBG based method with a virtual via-point, the spatio-temporal trajectories of the observed human reaching movements have been reproduced successfully.

Future research will be directed to investigate the influences of via-points on constrained human arm movements with consideration of environmental dynamics through a set of experimental and computational tests. Also, we plan to develop a design method of an optimal trajectory for guiding human movements operating a robotic system.

REFERENCES

1. F. Delcomyn, Neural basis of rhythmic behavior in animan, Science 210 (1980), 492–498.
2. T.G. Brown, On the nature of the fundamental activity of the nervous centers; together with an analysis of the conditioning of thythmic activity in progression, and a theory of evolution of function in the nervous system, Journal of Physiology 48 (1914), 18–46.
3. K. Matsuoka, Mechanisms of frequency and pattern control in the neural rhythm generators, Biol. Cybern. 56 (1987), 645–353.
4. G. Taga *et al.*, Self-organized control of bipedal locomotion by neural oscillators, Biol. Cybern. 65 (1991), 147–159.
5. O. Ekeberg, A combined neuronal and mechanical model of a fish swimming, Biol. Cybern. 66 (1993), 363–374.
6. A.J. Ijspeert, A connectionist central pattern generator for the aquatic and terrestrial gaits of a simulated salamander, Biol. Cybern. 84:(5) (2001), 331–348.
7. M. Suzuki, T. Tsuji, and H. Ohtake, A model of motor control of the nematode C. elegans with neuronal circuits, Artificial Intelligence in Medicine 2005 (in press).
8. S. Ito *et al.*, A model of adaptation to environmental changes in rhythmic movements, Transactions of the Society of Instrument and Control Engineers 34:(9) (1998), 1237–1245 (in Japanese).
9. S. Shcaal and D. Sternad, Programmable pattern generators, Proc the 3rd International Conference on Computational Intelligence in Neuroscience, 1998, pp. 48–51.
10. D. Sternad, W.J. Dean, and S. Shcaal, Interaction of rhythmic and discrete pattern generators in single-joint movements, Hum. Mov. Sci. 19 (2000), 627–664.
11. P. Morasso, Spatial control of arm movements, Exp. Brain Res. 42 (1981), 223–227.
12. T. Flash and N. Hogan, The coordination of arm movements: An experimentally confirmed mathematical model, Biol. Cybern. 57 (1985), 1688–1703.
13. M. Svinin, T. Odashima, Z.W. Luo, and S. Hosoe, On the optimization approaches to the trajectory formation of human movements, Proc the Complex Systems Intelligence and Modern Technological Applications, 2004, pp. 628–633.
14. Y. Uno, M. Kawato, and R. Suzuki, Formation and control of optimal trajectory in human multi-joint arm movement, Biol. Cybern. 61 (1989), 89–101.
15. C.M. Harris and D.M. Wolpert, Signal-dependent noise determines motor planning, Nature 394 (1998), 780–784.
16. D. Bullock and S. Grossberg, VITE and FLETE: Neural modules for trajectory formation and postural control, in Volitional Action, W.A. Hershberger (Editor), North-Holland/Elsevier, Amsterdam, 1989, pp. 253–297.
17. P. Morasso, V. Sanguineti, and T. Tsuji, A dynamical model for the generator of curved trajectories, Proc International Conference on Artificial Neural Networks, 1993, pp. 115–118.
18. T. Tsuji, P. Morasso, T. Yamanaka, and M. Kaneko, Feedback control of mobile robots with nonholonomic constraints using time base generator, Journal of the Robotics Society of Japan 12:(7) (1994), 1072–1078 (in Japanese).
19. T. Tsuji, P. Morasso, and M. Kaneko, Feedback control of nonholonomic mobile robots using time base generator, Proc IEEE International Conference on Robotics and Automation, 1995, pp. 1385–1390.
20. T. Tsuji, P. Morasso, V. Sanguineti, and M. Kaneko, Artificial force-field based methods in robotics, in Self-organization, computational maps and motor control, P. Morasso and V. Sanguineti (Editors), Advances in

Psychology, North-Holland/Elsevier, Amsterdam, 1997, pp. 169–190.
21. Y. Tanaka, T. Tsuji, and M. Kaneko, Dynamic control of redundant manipulators using the artificial potential field approach with time scaling, Journal of Artificial Life and Robotics 3 (1999), 79–85.
22. T. Tsuji, Y. Tanaka, M. Kaneko, and H. Miyaguchi, A bio-mimetic rehabilitation aid for reaching movements using time base generator, International Journal of Machine Intelligence and Robotic Control 2:(4) (2000), 141–149.
23. T. Tsuji, Y. Tanaka, P.G. Morasso, V. Sanguineti, and M. Kaneko, Bio-mimetic trajectory generation of robots via artificial potential field with time base generator, IEEE Transactions on Systems, Man, and Cybernetics—Part C: Applications and Reviews 32:(4) (2002), 426–439.
24. T. Tsuji, Y. Tanaka, and M. Kaneko, Biomimetic trajectory generation based on human movements with a nonholonomic constraint, IEEE Transactions on Systems, Man, and Cybernetics—Part A: Systems and Humans 32:(6) (2002), 773–779.
25. A. Mathew and M. Cook, The control of reaching movements by young infants, Child Dev. 61:(4) (1990), 1238–1257.
26. B. Fallang, O.D. Saugstad, and M. Hadders-Algra, Goal directed reaching and postural control in supine position in healthy infants, Behav. Brain Res. 115 (2000), 9–18.
27. M. Zak, Terminal attractors for addressable memory in neural networks, Phys. Lett. A 133 (1988), 218–222.
28. M. Sampei and K. Furuta, On time scaling for nonlinear systems: Application to linearization, IEEE Transactions on Automatic Control AC-31:(5) (1986), 459–462.
29. R.B. Salter, Clinical application of basic research on continuous passive motion for disorders and injury of synovial joints: A preliminary report of a feasibility study, J. Orthop. Res. 3 (1984), 325–342.
30. T. Sakaki, M. Kondo, K. Nagata, K. Matsukuma, and T. Sakamoto, Multi D.O.F. and force-controlled rehabilitation devices for human legs, Proc the 13th Annual Conference of Robotic Society Japan, 1995, pp. 1039–1040 (in Japanese).
31. Y. Okajima, N. Tanaka, M. Hasegawa, N. Uchida, A. Kimura, Y. Tomita, T. Horiuchi, M. Kondo, and T. Sakaki, Therapeutic exercise machine: Soft motion by the impedance control mechanism, Sogo Rehabilitation 26:(4) (1998), 363–369 (in Japanese).
32. H.I. Krebs, N. Hogan, M.L. Aisen, and B.T. Volpe, Robot-aided neurorehabilitation, IEEE Trans. Rehabil. Eng. 6:(1) (1998), 75–87.